Negative Longitudinal Piezoelectricity Coexisting with both Negative and Positive Transverse Piezoelectricity in Hybrid Formate Perovskite

Partha Sarathi Ghosh,*,†,‡ Sergey Lisenkov,¶ and Inna Ponomareva¶

†*Glass & Advanced Materials Division, Bhabha Atomic Research Centre, Mumbai 400 085, India*

‡*Homi Bhabha National Institute, Anushaktinagar, Mumbai 400 094, India*

¶*Department of Physics, University of South Florida, Tampa, Florida 33620, USA*

E-mail: psghosh@mail.usf.edu

Abstract

Negative longitudinal piezoelectric response is a rare property, which has been found mostly in inorganic materials. We use first-principles density functional theory simulations to predict such an unusual response in $[NH_2NH_3]Co(HCOO)_3$ - a representative of a large family of hybrid organic-inorganic formate perovskites. A feature that sets aside $[NH_2NH_3]Co(HCOO)_3$ from inorganic compounds with negative longitudinal piezoelectric response is that this rare property coexists with both negative and positive transverse piezoelectric response, which is highly desirable for tunable applications. Atomistic analysis reveals that this unusual electromechanical coupling originates from the high anisotropy of materials response to uniaxial stress. Such deformation produces oxygen octahedral tilts in the framework, whose magnitude depends strongly on the direction of the applied strain. For hard directions, the tilts make the dominant contribution to the deformation-induced change in polarization, while for

softer direction it is the tilts of the $NH_2NH_3^+$ cation that dominate the polarization response. The latter occur as the complex hydrogen bond network responds to the octahedra tilts. As high anisotropy of mechanical properties is a common feature across the formate perovskites we expect our findings to stimulate more discoveries of unusual electromehcanical couplings in this family.

Keywords: negative piezoelectric coefficients, uniaxial stress, uniaxial strain, hybrid organic-inorganic perovskites, first-principles calculations

Introduction

Piezoelectricity refers to the linear coupling between mechanical stress, X, and electric polarization, P, (the direct piezoelectric effect) or between mechanical strain and applied electric field (the converse piezoelectric effect). The typical value ranges from 1 pC/N in quartz to 1000 pC/N for PZT.[1] Mathematically, in matrix form the relation is $P_i = d_{ij}X_j$, where i and j are cartesian components. The longitudinal coefficient d_{ii} quantifies the change of polarization in the direction of the applied stress and is of practical significance.[2] In ferroelectrics, the longitudinal coefficient is typically referred to the response along the polar axis. In addition, d_{33} coefficient is the most accessible from the experimental measurements.[3]

Inorganic perovskites with ABO_3 formula unit, such as solid solution $Pb(Zr,Ti)O_3$, or PZT, are among the best piezoelectric materials. Their longitudinal piezoelectric coefficient is positive, i.e., the polarization increases along the direction of stretch and decreases along the compressed direction. The typical mechanism is that the expansion along certain direction increases ionic charge separation thus enhancing the polarization, and vice verse. Negative longitudinal piezoelectricity (NLPE), on the other hand, is quite rare. Experimentally only few materials have been demonstrated to possess NLPE: ferroelectric polymer poly(vinylidene fluoride) and its co-polymers,[4,5] two-dimensional layered ferroelectric

$CuInP_2S_6$,[6] some samples of hafnia.[7] A groundbreaking computational work predicted that materials of hexagonal ABC family of inorganic ferroelectrics can exhibit NLPE with values reaching -19 pC/N,[8] while the data-mining strategy revealed many more compounds with NLPE among hypothetical and synthesized materials. It was stressed that the sign of the coefficient arises from the interplay between the two terms: clamped-ion term, which quantifies the electronic response to strain, and internal strain contribution, which arises from the ionic response. In the ABC ferroelectrics with NLPE, the negative clamped-ion term dominates the total response, whereas the internal-strain contribution (positive for most compounds) is not large enough to compensate for that.[8] Moreover, it was predicted that ferroelectrics with NLPE coefficients show anomalous pressure-enhanced ferroelectricity.[8] Another first-principles study predicted negative piezoelectric response in van der Waals layered bismuth tellurohalides.[9] It was found that the structure within each triple layer of the materials is only weakly affected by the external stress, while the changes in the charge distribution under stress produce a substantial negative piezoelectric response. Therefore, NLPE in both families of materials[8,9] was predicted to originate from electronic effects. These trends have been generalized in another first-principles study, which reported anomalous NLPE in $CuInP_2S_6$ attributed to negative clamped-ion term uncompensated by the positive internal-strain part.[10] It was proposed that a negative clamped-ion term should be universal among piezoelectric materials, which is attributed to the "lag of Wannier center" effect.

NLPE coexisting with exotic electric auxetic effect was predicted in ferroelectric orthorhombic $Pca2_1$ phase of HfO_2 from first-principles computations in a recent study.[11] The effect originates from the domination of the negative internal-strain contribution over the positive clamped-ion contribution. NLPE in hafnia was later confirmed in a combined computational-experimental study,[7] although experimentally it was found to be sample dependent. It was also concluded that the internal strain contribution is responsible for the sign of the longitudinal piezoelectric coefficient. NLPE was recently predicted in interlayer-sliding ferroelectric ZrI_2,[12] while NLPE arising from the negative ionic contribution was also

predicted for ferromagnetic 1H-$LaBr_2$ monolayer.[13]

Interestingly, majority of the aforementioned predictions and experimental demonstrations involve inorganic compounds. A few exceptions are poly(vinylidene fluoride) and its co-polymers,[4,5] and an organic supramolecular ferroelectric BTAs (trialkylbenzene-1,3,5-tricarboxamides), in which, however, NLPE was attributed to defects.[14] One open question is whether hybrid organic-inorganic materials could exhibit NLPE. Among such materials hybrid organic-inorganic perovskites could be likely candidates as not only they have already demonstrated remarkable diversity of properties[15–17] and established their potential for piezoelectric mechanical energy harvesting[18] but also were predicted to exhibit enhancement of polarization under pressure,[19] which for inorganic materials was found to coexist with NLPE.[8] If indeed such unusual property can be found in hybrid organic-inorganic perovskites, would it originate from the mechanisms similar to the ones established for the inorganic materials or could they exhibit a completely different one? Could the piezoelectric response in such hybrid materials present other exotic trends? The goal of our study is to provide an atomistic first-principles insight into the answers to these questions using $[NH_2NH_3]Co(HCOO)_3$ as one representative from a large family of formate perovskites. In particular, we aim (i) to predict NLPE in this material; (ii) to report the rare coexistence of positive and negative transverse piezoelectricity in the same material; (iii) to reveal the atomistic origin of such unusual electro-mechanical response; and (iv) to predict pressure enhanced piezoelectricity in this material.

Methodology

All the electronic structure calculations are performed using a plane wave based spin-polarized density functional theory (DFT) as implemented in Vienna Ab-intio Simulation package (VASP).[20,21] The electron-ion interactions are described by projector augmented wave (PAW) potential[22] which includes the valence states of Co ($3d^8\ 4s^1$), O ($2s^2\ 2p^4$),

N ($2s^2$ $2p^3$) , C ($2s^2$ $2p^2$) and H ($1s^1$). The generalized gradient approximation (GGA) with Perdew-Burke-Ernzerhof (PBE) parameterization[23] is used for the exchange-correlation part. The Hubbard U correction for Co-d states are introduced using the method proposed by Dudarev *et al.*[24] The value we employed were U_{eff}= 2.0 eV as proposed in previous studies.[25,26] The van der Waals interactions are incorporated within the GGA using zero-damping DFT-D3 method of Grimme *et al.*[27] The choice of GGA+U+D3 has previously been shown to provide close agreement with experimental structural parameters for the case of $[NH_2NH_3]Co(HCOO)_3$.[28–30] A Monkhorst-Pack[31] k-space mesh of 5 × 5 × 3 in reciprocal space is used for the Brillouin zone integration. The plane wave cutoff energy of 700 eV for basis set was used throughout the simulation. The cohesive energies are optimized with respect to volume (or lattice parameter) and atomic positions using conjugate gradient algorithm until the residual forces and stress were less than 0.001 eV/Å and 0.1 GPa, respectively. The crystal polarization is evaluated by the Berry phase method developed by King-Smith and Vanderbilt.[32] Piezoelectric stress constants are calculated using density-functional perturbation theory (DFPT)[33] as implemented in the VASP package.

Results and Discussions

Experimentally $[NH_2NH_3]Co(HCOO)_3$ undergoes structural phase transition from nonpolar Pnma to polar $Pna2_1$ phase around 343 K.[34] The high temperature high symmetry phase is associated with the dynamical disorder of the cation. Here we focus on low temperature $Pna2_1$ phase and apply strain along either a, b or c crystallographic direction. Relaxations of lattice parameters are performed along the other two crystallographic directions and atomic positions are relaxed in all three directions. Such relaxation results in uniaxial stress along the constrained direction, while other components of the stress tensor σ_j are null. This corresponds to condition of uniaxial stress. We investigated a range of applied strain from -0.08 to 0.08 in steps of 0.02. The associated stress is taken as negative of the internal stress

value outputted by VASP. For each investigated value of strain we initialized simulations with DFT+U+D3 optimized ground state structure[30,35] and then carried out structural relaxation in either G-type antiferromagnetic (AFM) or ferromagnetic (FM) configuration. We also carried out additional calculations where the applied strain was sequentially decreased/increased in steps 0.02 from the zero value with each new simulation initialized by the output of the previous one. Both initialization strategies resulted in very similar relaxed structure.

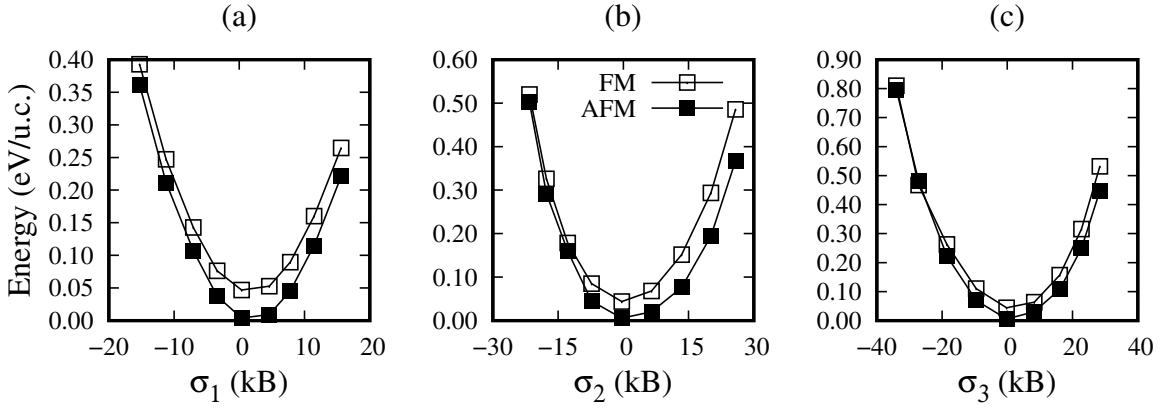

Figure 1: Relative energy as a function of uniaxial stress σ_i ((a)-(c)) for different magnetic configurations.

Figure 1 reports the energy dependence on stress computed at zero Kelvin for both AFM and FM configurations. We find that for all stresses in the given range the two magnetic configurations are very close in energy with AFM being just slightly lower. AFM configuration is therefore assigned as the magnetic ordering of the ground state.

Figure 2 presents the stress evolution of the volume and lattice parameters. In all cases we find that compression along one direction results in expansion along the other two and vice-versa for tension, as expected for a material with positive Poisson ratio.[28] The evolution of the lattice parameters with stress is smooth and suggests no stress induced structural phase transition at low temperatures. The structure remains in $Pna2_1$ space group. In all cases the volume of the structure decreases (increases) in response to compression (tension) in agreement with previous findings.[36] We find strong anisotropy in $V(\sigma_i)$ dependencies.

Namely, for the σ_2 stress the volume changes very little as compared with σ_1 and σ_3. Note that σ_2 is associated with [010] direction, which was previously found to exhibit negative linear compressibility under isotropic pressure.[28,29] The stress-strain dependencies are linear in all cases and given in Figure S1 (a) of Supporting Information. Furthermore, there exists anisotropy in the transverse deformations for the case of σ_1 and σ_2 stresses. For the case of σ_3, however, the transverse deformations are comparable. This is consistent with high anisotropy of Poisson ratio for deformations along [100] and [010] axes, predicted in Ref.[28] The evolution of Poisson ratios with strain along with its comparison with the zero strain values is presented in Figure S3 of Supporting Information.

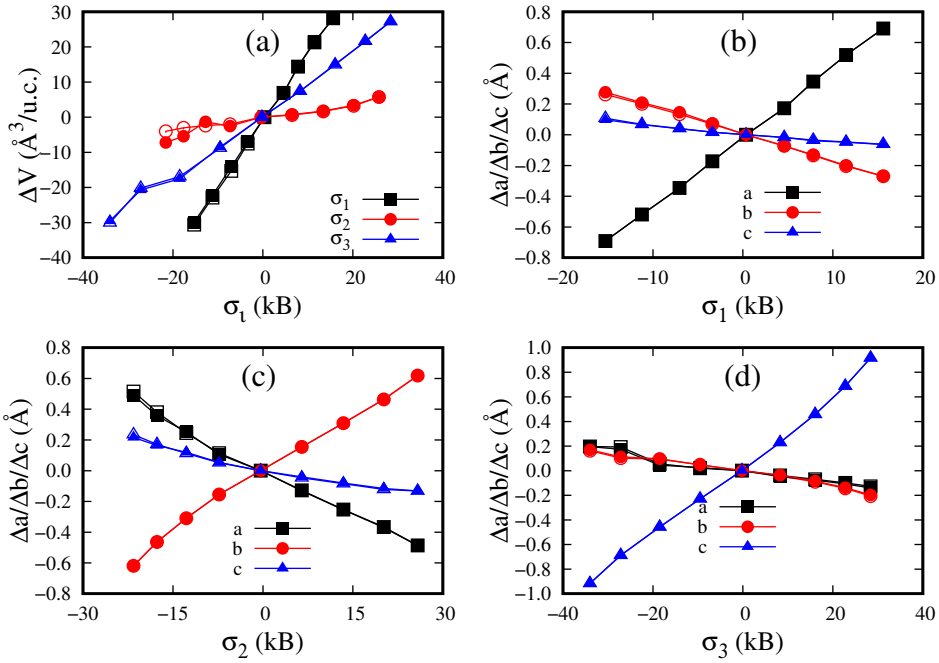

Figure 2: Dependence of relative change in volume (a) and change in lattice parameters (b)-(d) on uniaxial stress σ_i. Solid and empty points represent AFM and FM configurations, however, they mostly overlap.

Next we compute polarization for each stressed structure and report it in Figure 3 (a)-(c). Note, that we have previously verified the value of spontaneous polarization by constructing polarization reversal path[30] so the values reported here do not suffer from the uncertainty due to polarization quantum. As consistent with the space group $Pna2_1$ polarization is along [001] direction and is 2.56 μC/cm^2 in magnitude. Figure 3 (c) predicts that $P(\sigma_3)$ exhibits negative

slope, that is NLPE, which is, to the best of our knowledge, has not been reported for hybrid organic-inorganic perovskites. Figure 3 (b) predicts positive transverse piezoelectricity for σ_2, which is consistent with the NLPE. This could be further understood by inspection of the dependence of the polarization on the c-lattice parameter, which is displayed on top x-axis in Figure 3. Indeed, in both cases of σ_2 and σ_3 stresses, the dependence of $P(c)$ exhibits negative slope [compare Figure 3 (b) and (c)]. Interestingly, the situation is different for the other transverse response, shown in Figure 3(a), where we find that the slope $P(c)$ is positive resulting in negative transverse piezoelectricity when stressed along [100] axis. Thus, our calculations predict that in $[NH_2NH_3]Co(HCOO)_3$ both positive and negative transverse piezoelectricity coexists. We are not aware of other material that exhibit such an unusual property.

To estimate the effective piezoelectric response in the entire strain/stress range investigated we compute the slopes of the linear fits for $P(\sigma_i)$ dependencies. The slopes are $\partial P/\partial\sigma_1$ =-3.18, $\partial P/\partial\sigma_2$ =3.0, and $\partial P/\partial\sigma_3$ =-2.12 pC/N and comparable to piezoelectric response of inorganic materials.[8]

Another important aspect of electromechanical response is the response of polarization to uniaxial strain. To find out if such response also exhibits the aforementioned unusual features we repeated simulations but now without allowing lattice to relax in the directions perpendicular to the applied strain. We obtained the dependencies $P(\eta_i)$ similar to the ones reported in Figure 3(a)-(c) and provide them in Supporting Information (Figure S2) along with associated stress-strain dependencies (Figure S1 (b)). These allow us to conclude that the unusual features of the polarization response identified for uniaxial stress conditions persists under the condition of uniaxial strain also. The slopes $\partial P/\partial\eta_i$ under condition of uniaxial strain estimate "effective" piezoelectric stress coefficients e_{3i}. They are $\partial P/\partial\eta_1$ = -4.35, $\partial P/\partial\eta_2$ = 7.37, $\partial P/\partial\eta_3$ =-8.92 μC/cm^2 and listed in Table 1.

To compare this effective response with the usual zero strain piezolectric stress coefficients we computed the latter using DFPT and report the values in Table 1. Note, that DFPT is

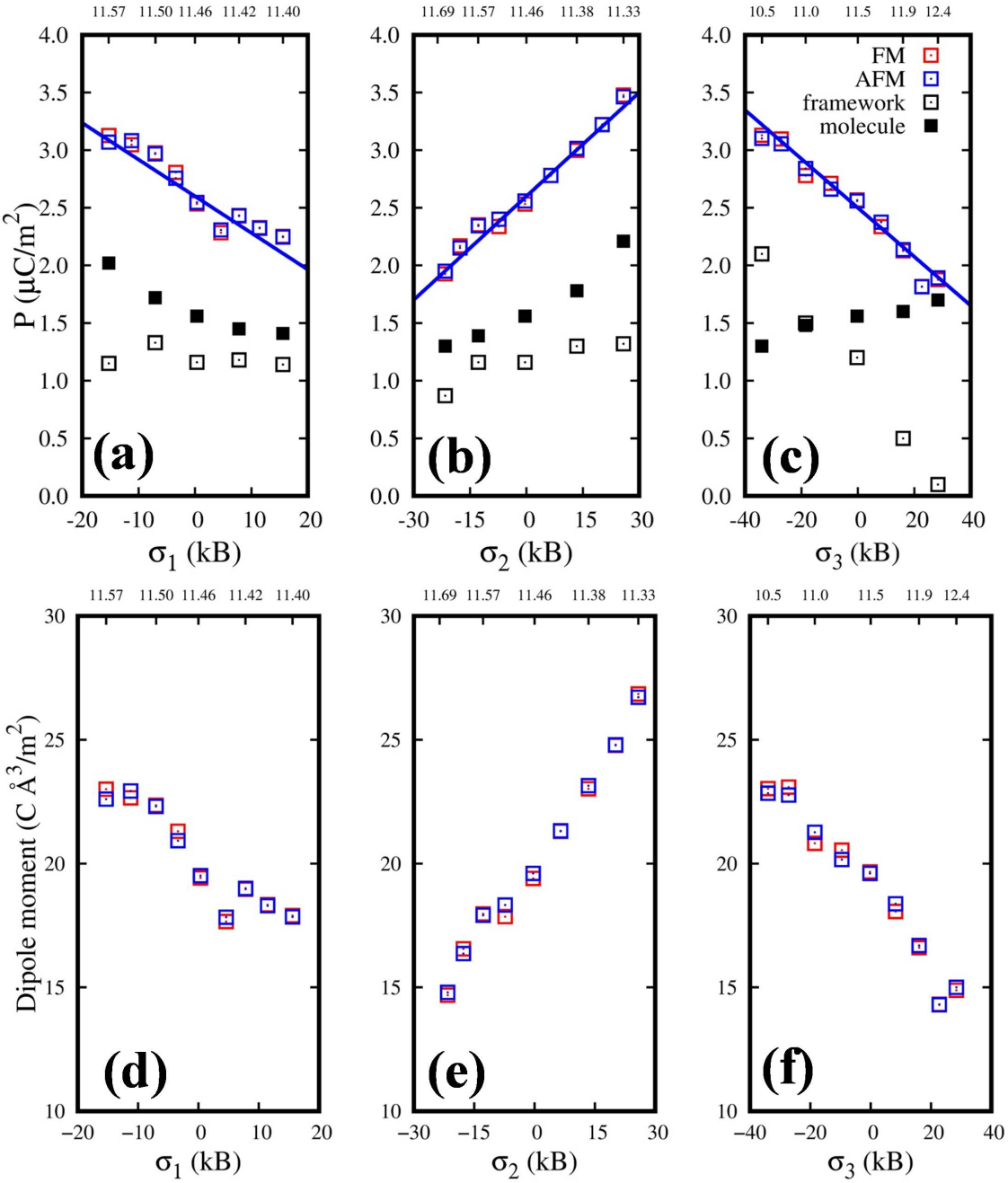

Figure 3: Dependence of polarization on uniaxial stress σ_1 (a), σ_2 (b), and σ_3 (c) for different magnetic configurations. Top x-axis on the graphs give c-lattice parameter. Solid lines are the linear fit of the data. Black open (closed) symbols give contributions from the framework (molecules) only. Dependence of the supercell dipole moment on uniaxial stress σ_1 (d), σ_2 (e), and σ_3 (f) for different magnetic configurations.

presently not implemented with D3 corrections so the corrections have been omitted in this calculation. It was mentioned previously that vdW-corrected functionals are best suited for structure optimization but not for calculating the electronic structure and phonons.[37] Just for comparison purposes we have also added the piezoelectric coefficients values computed for the ground state obtained using GGA+U only, that is without D3 corrections. The values are also listed in Table 1. The comparison of the data reveal that they all agree in the sign of both longitudinal and transverse piezoelectric response. Note, that the values are not expected to compare quantitatively, as DFTP constants are zero strain derivatives, while our effective response gives the slope in a wide range of strains. The advantage of DFPT calculations is that they allow to decompose the response into clamped-ion and relaxed-ion part. In agreement with Ref[8] we find that the clamped-ion response is negative for e_{33}. Interestingly, the relaxed-ion contribution to the same coefficient is also negative in contrast to the case of hexagonal ABC compounds.[8]

Table 1: Components of piezoelectric stress tensor e_{ij} (μC/cm^2) calculated using DFTP (top two panels of the Table) and the slopes $\frac{\partial P}{\partial \eta_i}$ and $\frac{\partial P}{\partial \sigma_i}$ computed from the $P(\eta_i)$ or $P(\sigma_i)$ dependencies reported in Figure 3 and in Figure S2 of Supporting Information.

	e_{15}	e_{24}	e_{31}	e_{32}	e_{33}
GGA+U+D3 computed ground state					
clamped-ion	2.96	0.66	3.71	1.28	-3.56
relaxed-ion	-10.75	5.44	-3.81	3.14	-1.60
total	-7.79	6.10	-0.10	4.42	-5.16
GGA+U computed ground state					
clamped-ion	2.63	0.25	3.53	0.95	-3.72
relaxed-ion	-8.75	8.30	-6.18	3.69	-3.71
total	-6.12	8.55	-2.65	4.64	-7.43
Uniaxial Stress (pC/N)					
Volume change contribution $-\frac{P_0}{V_0}\frac{\partial V}{\partial \sigma_i}\|_{\sigma_i=0}$	-	-	-0.64	-0.06	-0.31
Dipole moment change contribution $\frac{1}{V_0}\frac{\partial p}{\partial \sigma_i}\|_{\sigma_i=0}$	-	-	-2.50	3.07	-1.94
$\frac{\partial P}{\partial \sigma_i}$	-	-	-3.18	3.00	-2.24
Uniaxial Strain (μC/cm^2)					
Volume change contribution $-\frac{p_0}{V_0} = -P_0$	-	-	-2.59	-2.53	-2.49
Dipole moment change contribution $\frac{1}{V_0}\frac{\partial p}{\partial \eta_i}\|_{\eta_i=0}$	-	-	-1.81	9.85	-6.50
$\frac{\partial P}{\partial \eta_i}$	-	-	-4.35	7.37	-8.92

To investigate further into the origin of such unusual response we turn to the role of volume change in stressed supercell. As hybrid perovskites are structurally soft, they may exhibit relatively large changes in volume when mechanically stressed. Because the polarization is defined as the dipole moment, p, per unit volume, $P = p/V$, the large volume variations will have a strong imprint in the polarization, and consequently, piezoelectric coefficients. Indeed, in Ref.[19] it was found that the change of polarization under pressure is mostly due to change in the volume, while the dipole moment remains almost constant. Figure 3(d)-(f) shows dependence of the dipole moment on uniaxial stress, which is qualitatively similar to the polarization dependence on the strain, suggesting that the slopes of $P(\sigma_i)$ originate from the stress evolution of the dipole moment.

To quantify the effect of volume change we follow Ref.[9] and decompose both e_{3i} and d_{3i} into two terms, one originating from the change in volume, while the other from the change in the dipole moment. The expressions are $e_{3i} = -P_0 + \frac{1}{V_0}\frac{\partial p}{\partial \eta_i}|_{\eta_i=0}$ and $d_{3i} = -\frac{P_0}{V_0}\frac{\partial V}{\partial \sigma_i}|_{\sigma_i=0} + \frac{1}{V_0}\frac{\partial p}{\partial \sigma_i}|_{\sigma_i=0}$ where P_0 and V_0 are the spontaneous polarization and the supercell volume, respectively, at zero strain/stress. The first term in both expressions provides negative contribution as the decrease/increase of volume condenses/dilutes polarization. Linear fit of $p(\eta_i)$ under uniaxial strain gives $\frac{1}{V_0}\frac{\partial p}{\partial \eta_i}|_{\eta_i=0}$= -1.81, 9.85, and -6.50 μC/cm^2 for η_1, η_2, and η_3, respectively, which are also summarized in Table 1. These values either dominate over or are comparable to the spontaneous polarization contribution of -2.56 μC/cm^2 so we conclude that the NLPE as well as the unusual transverse responses do not originate primarily from the volume evolution under uniaxial strain. It is the change in the dipole moment under strain that make the dominating contribution into the piezoelectric response in case of η_2 and η_3 uniaxial strains (see Table 1). For the case of uniaxial stress the slopes are listed in Table 1 and demonstrate that volume change makes insignificant contribution to the piezoelectric strain response, which is dominated by the change in the dipole moment.

To further investigate into the origin of NLPE we decompose the polarization evolution under uniaxial stress into contributions from the $Co(HCOO)_3$ framework and from the

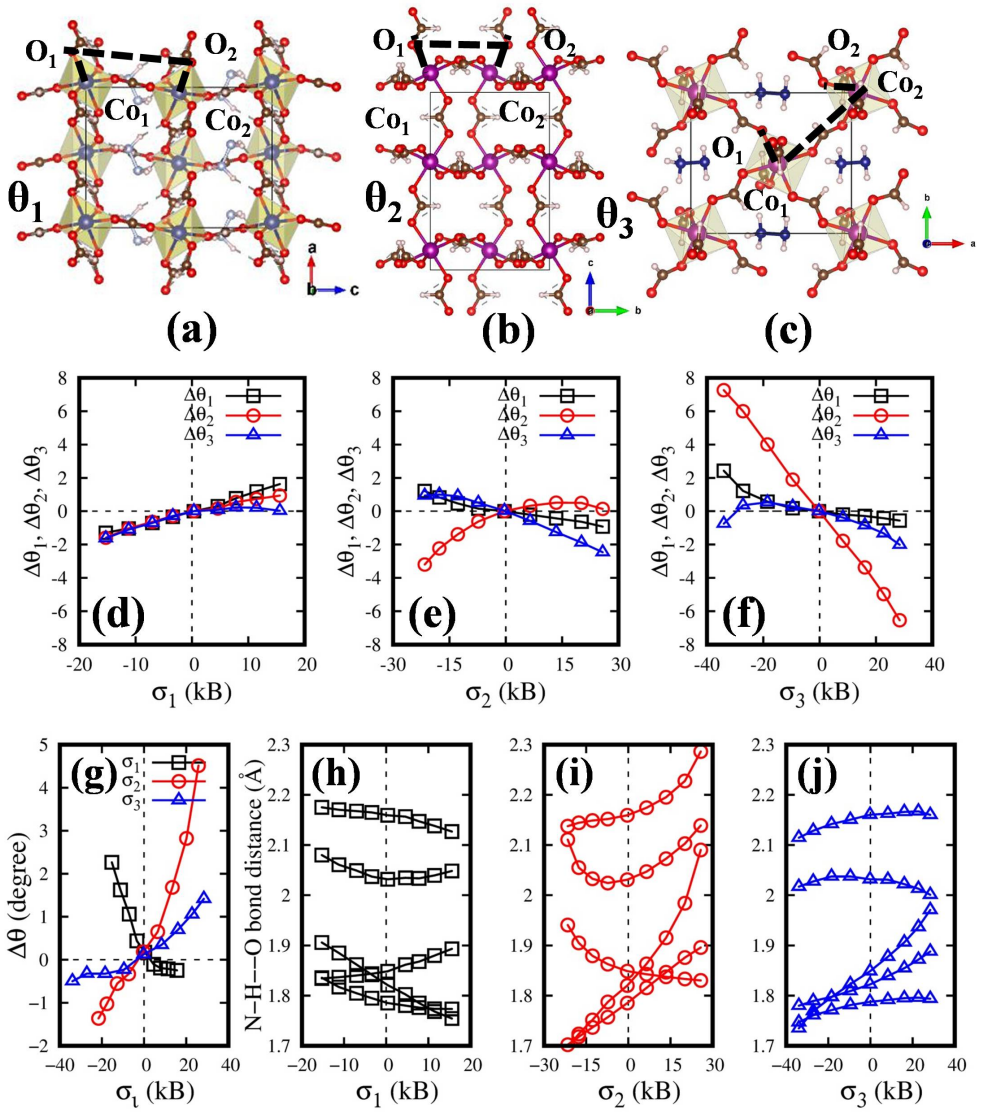

Figure 4: Crystal structure of $[NH_2NH_3]Co(HCOO)_3$ in different planes showing different dihedral angles, θ_i, formed by Co_1-O_1-O_2-Co_2 (a)-(c). The stress evolution of different dihedral angles change $\Delta\theta_i$ with respect to zero stress values (d)-(f). The change in the tilting angle of $[NH_2NH_3]$ molecule, $\Delta\theta$, with respect to the zero stress value as a function of uniaxial stress (g). Variation of N-H–O H-bond lengths as a function of uniaxial stress (h)-(j).

$[NH_2NH_3]$ molecule. Technically, we first keep the framework at its zero strain configurations while allowing the $[NH_2NH_3]$ molecule to evolve along the same trajectory as in the original calculations reported in Figure 3. This allows to trace the contribution of the molecule reorientation to the polarization. Next we keep the molecules at their zero strain configura-

tion, while allowing the framework to evolve as in the original calculations. This quantifies the contribution of the framework to the polarization evolution. Firstly, we notice that the framework makes very small contribution to the polarization evolution in case of σ_1 and σ_2 stresses. The situation is reversed, however, for the case of σ_3, where the framework contribution dominates the polarization evolution under stress. This can be explained by the fact the the [001] direction is the direction of $HCOO^-$ ligand and one of the hardest directions of the material ([110] is the other one).[28,29] It was previously found that along this direction pressure is accommodated through CoO_6 octaherda tilts.[28,29] Consequently, such tilts bring about significant change in the framework contribution to the polarization. In fact, it is the contribution from the framework that is responsible for the NLPE in this material. For the σ_1 and σ_2 stresses it is the molecular contributions, which are responsible for the sign of the piezoelectric response. The slopes for the molecular responses in these two cases have different signs, which explains the difference in the sign of the transverse piezoelectric coefficients. In Figure 3 we report data for both FM and AFM magnetic configurations, however, no significant differences in the values are found.

To further understand these trends we turn to the structural response of stressed supercells. Figure 4 gives CoO_6 octahedral and $[NH_2NH_3]$ molecular tilts with respect to their zero stress configurations. We quantify the CoO_6 octahedra tilts by the change in the Co_1-O_1-O_2-Co_2 polyhedral angles with respect to zero stress value [Figure 4(d)-(f)]. The angles are shown schematically in Figure 4(a)-(c). The data reveal that the CoO_6 octahedra tilts are largest in case of σ_3 uniaxial stress and significantly smaller in other two cases. This is consistent with our observation in Figure 3(c) that framework contribution dominates the polarization evolution when stressed in c direction. Figure 4(g) reveals that the slope of the molecular tilts is correlated with the the slope of the molecular contribution into $P(\sigma_i)$ dependencies (see Figure 3), which suggests that the latter originates from the molecular tilts. Furthermore, the largest molecular tilts are found for σ_2 stress followed by σ_1 and σ_3 ones, which correlates well with the strength of the molecular contribution to $P(\sigma_i)$. To

trace the origin of the molecular tilts we turn to the stress evolution of N-H–O H-bonding network shown in Figure 4(h)-(j) as this network is primarily responsible for the molecular orientation. Indeed, we find the largest distortion of the H-bond network for the case of σ_2 stress. This suggests that the distortion of the framework sets the molecular tilts into a motion through the H-bond network.

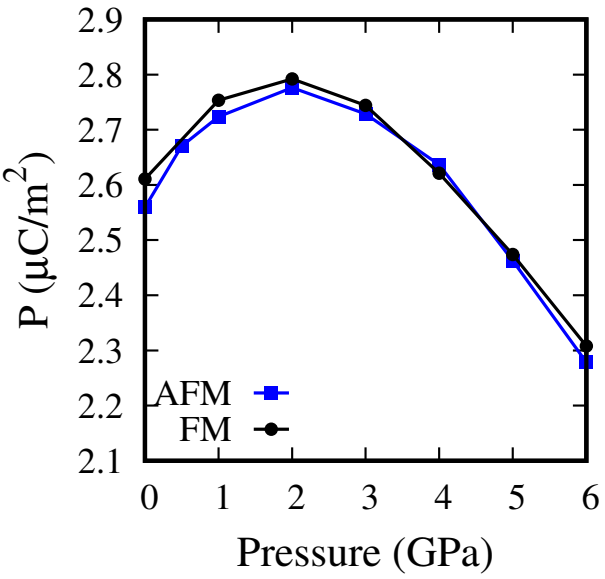

Figure 5: Dependence of polarization on hydrostatic pressure for FM and AFM configurations.

In Ref.[8] it was noted that in inorganic hexagonal materials NLPE coexists with anomalous pressure-enhanced ferroelectricity. To find out whether $[NH_2NH_3]Co(HCOO)_3$ can also exhibit such coexistence we computed polarization response to hydrostatic pressure and report it in Figure 5. Indeed, we find the enhancement of the polarization in the 0 to 2 GPa pressure range. Outside of this range polarization decreases as a function of hyrdostatic pressure. Our findings reveal that NLPE coexists with pressure-enhanced ferroelectricity in hybrid organic-inorganic perovskite.

Conclusions

In summary, we have used first-principles DFT computations to predict the unusual NLPE in hybrid organic-inorganic formate perovskites $[NH_2NH_3]Co(HCOO)_3$. Strikingly, this NLPE coexists with both positive and negative transverse piezoelectric response, which is highly desirable but so far elusive materials property. The origin of such exotic behavior is traced to highly anisotropic response of the octaherda framework to the mechanical deformations. Deformation along hard axes results in the oxygen octahedra tilts which make dominant contribution to the polarization evolution under strain. Deformations along soft axes, on the other hand, yield smaller distortions in the framework, which however are capable of tilting $[NH_2NH_3]$ molecules through the network of hyrdogen bonds. Such molecular tilts are responsible for the change in polarization in this case and could either enhance or suppress the polarization depending on their sense of rotation. The atomistic insight into the unique electromechanical response of the large family of perovskite formates does not only advance their fundamental understanding but could enable innovative design strategies for property optimization.

Acknowledgement

The work is supported by the National Science Foundation under the grant EPMD-2029800.

Supporting Information

Stress-strain dependencies from uniaxial stress/strain simulations, polarization vs. strain plots under uniaxial strain condition, Poission's ratios vs. strain plots under uniaxial stress conditions.

References

(1) Newnham, R. E. *Properties of Materials: Anisotropy, Symmetry, Structure*; Oxford University Press Inc., 2005.

(2) Uchino, K. *Ferroelectric Devices*, 3rd ed.; CRC Press, 2010.

(3) Cain, M. G. *Characterisation of Ferroelectric Bulk Materials and Thin Films*; Springer: Dordrecht, 2014.

(4) Katsouras, I.; Asadi, K.; Li, M.; van Driel, T. B.; Kjaer, K. S.; Zhao, D.; Lenz, T.; Gu, Y.; Blom, P. W. M.; Damjanovic, D.; Nielsen, M. M.; de Leeuw, D. M. The Negative Piezoelectric Effect of the Ferroelectric Polymer poly(vinylidene fluoride). *Nature Materials* **2016**, *15*, 78–84.

(5) Furukawa, T.; Wen, J. X.; Suzuki, K.; Takashina, Y.; Date, M. Piezoelectricity and Pyroelectricity in Vinylidene fluoride/trifluoroethylene Copolymers. *Journal of Applied Physics* **1984**, *56*, 829–834.

(6) You, L.; Zhang, Y.; Zhou, S.; Chaturvedi, A.; Morris, S. A.; Liu, F.; Chang, L.; Ichinose, D.; Funakubo, H.; Hu, W.; Wu, T.; Liu, Z.; Dong, S.; Wang, J. Origin of Giant Negative Piezoelectricity in a Layered Van der Waals Ferroelectric. *Science Advances* **2019**, *5*, eaav3780.

(7) Dutta, S.; Buragohain, P.; Glinsek, S.; Richter, C.; Aramberri, H.; Lu, H.; Schroeder, U.; Defay, E.; Gruverman, A.; Íñiguez, J. Piezoelectricity in hafnia. *Nature Communications* **2021**, *12*, 7301.

(8) Liu, S.; Cohen, R. E. Origin of Negative Longitudinal Piezoelectric Effect. *Phys. Rev. Lett.* **2017**, *119*, 207601.

(9) Kim, J.; Rabe, K. M.; Vanderbilt, D. Negative Piezoelectric Response of Van der Waals Layered Bismuth Tellurohalides. *Phys. Rev. B* **2019**, *100*, 104115.

(10) Qi, Y.; Rappe, A. M. Widespread Negative Longitudinal Piezoelectric Responses in Ferroelectric Crystals with Layered Structures. *Phys. Rev. Lett.* **2021**, *126*, 217601.

(11) Liu, J.; Liu, S.; Yang, J.-Y.; Liu, L. Electric Auxetic Effect in Piezoelectrics. *Phys. Rev. Lett.* **2020**, *125*, 197601.

(12) Ding, N.; Chen, J.; Gui, C.; You, H.; Yao, X.; Dong, S. Phase Competition and Negative Piezoelectricity in Interlayer-sliding Ferroelectric ZrI_2. *Phys. Rev. Materials* **2021**, *5*, 084405.

(13) Noor-A-Alam, M.; Nolan, M. Negative Piezoelectric Coefficient in Ferromagnetic 1H-LaBr2 Monolayer. *ACS Applied Electronic Materials* **2022**, *4*, 850–855.

(14) Urbanaviciute, I.; Meng, X.; Biler, M.; Wei, Y.; Cornelissen, T. D.; Bhattacharjee, S.; Linares, M.; Kemerink, M. Negative Piezoelectric Effect in an Organic Supramolecular Ferroelectric. *Mater. Horiz.* **2019**, *6*, 1688–1698.

(15) Hu, Y.; You, L.; Xu, B.; Li, T.; Morris, S. A.; Li, Y.; Zhang, Y.; Wang, X.; Lee, P. S.; Fan, H. J.; Wang, J. Ferroelastic-Switching-driven Large Shear Strain and Piezoelectricity in a Hybrid Ferroelectric. *Nature Materials* **2021**, *20*, 612–617.

(16) Li, W.; Probert, M. R.; Kosa, M.; Bennett, T. D.; Thirumurugan, A.; Burwood, R. P.; Parinello, M.; Howard, J. A. K.; Cheetham, A. K. Negative Linear Compressibility of a Metal-Organic Framework. *Journal of the American Chemical Society* **2012**, *134*, 11940–11943.

(17) Chen, X.-G.; Song, X.-J.; Zhang, Z.-X.; Li, P.-F.; Ge, J.-Z.; Tang, Y.-Y.; Gao, J.-X.; Zhang, W.-Y.; Fu, D.-W.; You, Y.-M.; Xiong, R.-G. Two-Dimensional Layered Perovskite Ferroelectric with Giant Piezoelectric Voltage Coefficient. *Journal of the American Chemical Society* **2020**, *142*, 1077–1082.

(18) Vijayakanth, T.; Liptrot, D. J.; Gazit, E.; Boomishankar, R.; Bowen, C. R. Recent Advances in Organic and Organic–Inorganic Hybrid Materials for Piezoelectric Mechanical Energy Harvesting. *Advanced Functional Materials* **2022**, *32*, 2109492.

(19) Ghosh, P. S.; Doherty, J.; Lisenkov, S.; Ponomareva, I. Tunability of Structure, Polarization, and Band Gap of High T_c Organic-Inorganic Ferroelectrics by Hydrostatic Pressure: First-Principles Study. *The Journal of Physical Chemistry C* **2021**, *125*, 16296–16303.

(20) Kresse, G.; Furthmüller, J. Efficient Iterative Schemes for Ab-initio Total-energy Calculations using a Plane-wave Basis Set. *Phys. Rev. B* **1996**, *54*, 11169–11186.

(21) Kresse, G.; Joubert, D. From Ultrasoft Pseudopotentials to the Projector Augmented-wave Method. *Phys. Rev. B* **1999**, *59*, 1758–1775.

(22) Blöchl, P. E. Projector Augmented-wave Method. *Phys. Rev. B* **1994**, *50*, 17953–17979.

(23) Perdew, J. P.; Burke, K.; Ernzerhof, M. Generalized Gradient Approximation Made Simple. *Phys. Rev. Lett.* **1996**, *77*, 3865–3868.

(24) Dudarev, S.; Botton, G.; Savrasov, S.; Humphreys, C.; Sutton, A. Electron-energy-loss Spectra and the Structural Stability of Nickel Oxide: An LSDA+U Study. *Phys. Rev. B* **1998**, *57*, 1505.

(25) Fung, V.; Tao, F. F.; en Jiang, D. Trends of Alkane Activation on Doped Cobalt (II, III) Oxide from First Principles. *Chem Cat Chem* **2018**, *10*, 244–249.

(26) Liu, J.; Zhang, S.; Zhou, Y.; Fung, V.; Nguyen, L.; Jiang, D.; Shen, W.; Fan, J.; Tao, F. F. Tuning catalytic selectivity of oxidative catalysis through deposition of nonmetallic atoms in surface lattice of metal oxide. *ACS Catal.* **2016**, *6*, 4218–4228.

(27) Grimme, S.; Antony, J.; Ehrlich, S.; Krieg, H. A Consistent and Accurate Ab-initio

Parametrization of Density Functional Dispersion Correction (DFT-D) for the 94 Elements H-Pu. *J. Chem. Phys.* **2010**, *132*, 154104.

(28) Ghosh, P. S.; Ponomareva, I. Negative Linear Compressibility in $[NH_3NH_2]Co(HCOO)_3$ and Its Structural Origin Revealed from First Principles. *J. Phys. Chem. Lett.* **2021**, *12*, 7560–7565.

(29) Ghosh, P. S.; Ponomareva, I. Negative Linear Compressibility in Organic–Inorganic Hybrid Perovskite $[NH_2NH_3]X(HCOO)_3$ (X = Mn, Fe, Co). *The Journal of Physical Chemistry Letters* **2022**, *13*, 3143–3149.

(30) Ghosh, P. S.; DeTellem, D.; Ren, J.; Witanachchi, S.; Ma, S.; Lisenkov, S.; Ponomareva, I. Unusual Properties of Hydrogen-Bonded Ferroelectrics: The Case of Cobalt Formate. *Phys. Rev. Lett.* **2022**, *128*, 077601.

(31) Monkhorst, H. J.; Pack, J. D. Special Points for Brillouin-zone Integrations. *Phys. Rev. B: Condens. Mater. Phys.* **1979**, *13*, 5188.

(32) King-Smith, R. D.; Vanderbilt, D. Theory of Polarization of Crystalline Solids. *Phys. Rev. B* **1993**, *47*, 1651–1654.

(33) Gajdoš, M.; Hummer, K.; Kresse, G.; Furthmüller, J.; Bechstedt, F. Linear Optical Properties in the Projector-Augmented Wave Methodology. *Phys. Rev. B* **2006**, *73*, 045112.

(34) Gunatilleke, W. D. C. B.; Wei, K.; Niu, Z.; Wojtas, L.; Nolas, G.; Ma, S. Thermal Conductivity of a Perovskite-type Metal-Organic Framework Crystal. *Dalton Trans.* **2017**, *46*, 13342–13344.

(35) Ghosh, P. S.; Lisenkov, S.; Ponomareva, I. NH_2NH_3-$Co(HCOO)_3$ Experimental Structures and DFT+U+D3 Optimized Structures. 2021; `https://github.com/USFmatscilab/NH2NH3-Co-HCOO_3`.

(36) Durandurdu, M. Structural Phase Transition of Germanium Under Uniaxial Stress: An Ab Initio Study. *Phys. Rev. B* **2005**, *71*, 054112.

(37) Marom, N.; Tkatchenko, A.; Scheffler, M.; Kronik, L. Describing Both Dispersion Interactions and Electronic Structure Using Density Functional Theory: The Case of Metal-Phthalocyanine Dimers. *Journal of Chemical Theory and Computation* **2010**, *6*, 81–90.

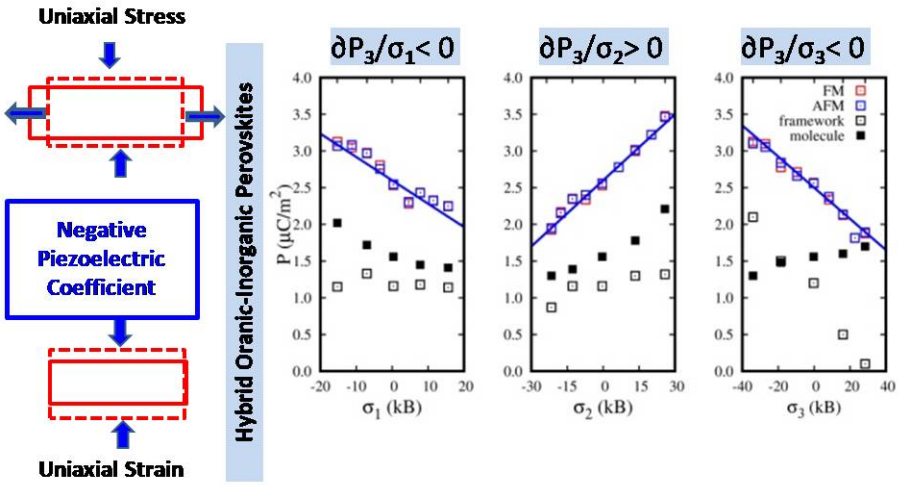
Uniaxial Stress
Negative Piezoelectric Coefficient
Uniaxial Strain
Hybrid Oranic-Inorganic Perovskites
∂P3/σ1< 0
∂P3/σ2> 0
∂P3/σ3< 0
P (μC/m2)
σ1 (kB)
σ2 (kB)
σ3 (kB)
FM
AFM
framework
molecule